Solar Energy 196 (2020) 196–206

Contents lists available at ScienceDirect

Solar Energy

journal homepage: www.elsevier.com/locate/solener

Degradation analysis of a photovoltaic generator after operating for 15 years in southern Brazil

José Eduardo Ferreira da Fonseca*, Fernando Schuck de Oliveira, César Wilhelm Massen Prieb, Arno Krenzinger

Federal University of Rio Grande do Sul, Brazil

ARTICLE INFO

Keywords:
Photovoltaic module performance
Degradation
Field performance
Reliability
Electroluminescence imaging
I-V curve testing

ABSTRACT

Photovoltaic modules long-term reliability is a key requirement to keep this technology a commercially interesting option for energy production. The investment return on PV generation system depends, among other factors, on the peculiarities of the system on efficiency reduction caused by environmental action. Technical standards suggest laboratory tests for the qualification and a better understanding on module degradation behavior. Nevertheless, some degradation modes can only be observed after years of field operation. This paper presents the main signs of degradation on crystalline silicon photovoltaic modules caused by outdoor exposure after a period of 15 years in an installation in the city of Porto Alegre, the southernmost state capital city in Brazil. The electric analysis demonstrated that the modules kept 90.5% of their initial power, with an average of degradation rate of 0.7% per year. Some techniques helped the evaluation of defects caused by exposure of the arrays for long periods of operation, such as electroluminescence imaging and *I-V* curve testing. The most frequent defects found were browning (encapsulant darkening) and cell encapsulant delamination, leading to the anti-reflective layer deterioration. The junction box of one of the modules was detached, allowing the entrance of moisture and resulting in the disconnection of some of the module cells. The electroluminescence technique also provided a better understanding on modes of degradation. Despite the observed evidences of degradation along these 15 years, it can be said that the system remains within the expected operation limits.

1. Introduction

In the last few years there has been a significant increase in electricity generation systems using photovoltaic technology. The installed capacity in 2018 grew by around 100 GW compared to the accumulated capacity until the previous year and the same occurred between 2016 and 2017. The world installed capacity is currently around 500 GW (IEA, 2019). Studies indicate that, considering a less conservative scenario, by 2022 the accumulated power will reach 1 TW (SPA, 2018). This growth is mostly due to the reduction on equipment costs. Besides, in 2017 photovoltaic systems had a greater increment of installed power than any other form of electricity production (REN21, 2018).

Considering the favorable scenario of photovoltaics among other renewable energies, energy production estimation must be more and more accurate to guarantee the investment return. In order to evaluate the feasibility of an installation at some intended site, historical meteorological data and modules degradation rate lead to reliable assessments and improve the estimation accuracy of the produced energy. An incorrectly determined modules power degradation rate may even menace the economic viability of a photovoltaic energy installation. A thorough understanding of module degradation mechanisms in field operation is required to make better use of the device during its lifetime (Chandel et al., 2015; IEC 61215-1, 2016).

In this context, the present work aims to evaluate the operation of a photovoltaic generator installed 15 years ago the city of Porto Alegre, located at the South of Brazil. The analysis of the predominant degradation mechanisms was based on studies and qualification standards. Finally, we expect to draw the relation between environmental conditions and the occurrence of these degradation mechanisms, besides determining the module degradation influence on the system electrical behavior.

1.1. Background

Degradation studies typically use indoor tests under specific conditions that provoke accelerated stresses. The qualification standards for photovoltaic devices are developed based on such studies. The qualification tests are performed mostly according to IEC (International

* Corresponding author.
E-mail addresses: ejosefonseca@gmail.com (J.E.F. da Fonseca), cprieb@ufrgs.br (C.W. Massen Prieb), arno.krenzinger@ufrgs.br (A. Krenzinger).

https://doi.org/10.1016/j.solener.2019.11.086
Received 27 August 2019; Received in revised form 22 November 2019; Accepted 25 November 2019
Available online 14 December 2019

Electro Technical) standard IEC 61215-1 (2016). Some of these tests aim to mimic the mechanisms of degradation. The standardized procedures helped to promote and ensure the durability of photovoltaic modules up to the present day (Osterwald and McMahon, 2009). However, these tests alone do not have the ability to reproduce all degradation modes observed in real-time field exposure (Jorgensen and McMahon, 2008). Accelerated tests apply stresses in predetermined sequences. Under real operating conditions, UV radiation, moisture and thermal stress are simultaneously applied and act synergistically, resulting in different defects or degradation modes. In addition, high voltages, wind, snow loads, hail, etc. can also cause premature (and in some cases) irreversible failures (Köntges et al., 2014).

For the accelerated tests listed in the qualification standards, thermal cycling and damp heat are, respectively, the most deleterious tests (Köntges et al., 2014). Wohlgemuth and Kurtz (2011) studied the impact of damp heat tests on modules submitted to 85 °C temperature and 85% relative humidity, indicating that corrosion appeared after 1000 h of exposure. Zhu et al. (2016) evaluated the influence of accelerated tests on specific damp heat conditions for different modules over periods that exceeded the standard recomendations. They observed that overexposure to temperature and heat can induce the growth of inactive areas in some modules, compromising the electric performance. These processes were detected through electroluminescence (EL) imaging. This technique can reveal how the metal contacts degradation occurs in both accelerated tests and field operating conditions under humid environments, a condition that can induce corrosion of the module components.

In the context of the extensive range of damage scenarios that affect photovoltaic modules, Berardone et al. (2018) points that there are still few studies employing EL and infrared (IR) imagery. The application of these two techniques has advantages and drawbacks and a combined use has not been extensively made. EL may indicate intrinsic defects such as grain boundaries, dislocations, shunts, or process failures, as well as extrinsic defects such as cracks and interrupted contacts (Bedrich et al., 2018; Harvey et al., 2016). On the other hand, IR techniques can indicate the existence of hot-spots, besides showing the temperature distribution pattern.

Studies on photovoltaic modules degradation carried out over the last 40 years show that the mean power degradation rate in c-Si modules is 0.7% per year and a median of 0.5% per year (Jordan et al., 2013). Most photovoltaic systems have been installed in the last five years (IEA, 2019), so for newly developed cell technology modules there are no long-term performance records, reinforcing the importance of these studies. Furthermore, there is little information on PV modules degradation modes in terms of frequency, evolution rate and level of impact on module lifetime and reliability (Ndiaye et al., 2013). Different cell technologies, module materials, local aspects (such as humidity, yearly number of sunshine hours, among others) have influence photovoltaic systems degradation (Jordan et al., 2012; Schweiger et al., 2017). Some environmental conditions may favor a better use of local energy resources in photovoltaic installations. In contrast, some specific types of defects may be related to specific climatic conditions (Jordan et al., 2017; Larocca, 2013).

Modules manufacturers often guarantee a minimum performance for up to twenty-five years, indicated as a fraction of the initial value (between 70% and 80%) (Köntges et al., 2014). Such simplification aims to provide consumers with easy-to-understand warranty rules. Nevertheless, there are systems operating for a longer period than the limit defined by the warrantees (Chandel et al., 2015; Tang et al., 2006). During their life cycle, some problems may arise and affect the operation of the modules even without major influence on the behavior of the system and the energy production, such as EVA darkening, small delaminations (Lorenzo et al., 2013) and permanent dirt (VERA et al., 2006). Other problems, as hot-spots (García et al., 2013; Moretón et al., 2015; Rajput et al., 2018; Sánchez-Friera et al., 2011) and electrical insulation failure (Skoczek et al., 2009) may also occur during the operating life but affecting the electrical behavior and the system integrity. Some effects, such as broken cells, can be originated by external, environmental factors. Monitoring (Solórzano and Egido, 2013) and preventive maintenance are important tools to promote better use of energy resources, as well as understanding the different limitations of both the technologies and the locations with varying climatic conditions where the systems are installed.

In the initial period of operation, degradation rates tend to be higher than in the rest of the operating life due to the stronger action of specific degradation modes, such as LID (light induced degradation) (Ishii and Masuda, 2017; Osterwald et al., 2005; Pingel et al., 2010). The so called darkening, in turn (Osterwald et al., 2005), affects the systems during its mid-life period, reducing the I_{SC} (short circuit current) of the modules (Pern, 1996).

Chandel et al. (2015) evaluated the field degradation of 12 modules connected to a pumping system in the Indian Himalayan region, estimating a degradation rate of 1.4% per year after 28 years of operation. Also in India, Rajput et al. (2016a,b) examined a system composed by 90 modules after 22 years of operation, resulting in average losses of 1.9% per year.

The modules power degradation rate of photovoltaic system operating for 20 years in Ispra, Italy, was found to be 0.8% per year considering all the studied modules and slightly smaller (0.67%) when excluding faulty modules (Skoczek et al., 2009). Polverini et al. (2012), in the same region, found the degradation rate to be around 0.24% per year in a facility also with 20 years of operation. Lorenzo et al. (2013) reported an annual decrease of power of 0.53% in a 7 kW_P generator's modules after 17 years of operation in Madrid, Spain. Sánchez-Friera et al. (2011) indicate annual losses of 1% after 12 years in a 2 kW_P generator located in Malaga, Spain, noting that the initial effects of LID are included as well as anti-reflective layer damage, delamination and contacts corrosion.

Analyzing a system composed by 8 modules, in Porto Alegre (locality of the present study), an average 6% degradation in the power of the modules was evaluated after 6 years of operation, that is, approximately 1% per year (VERA et al., 2006). The authors emphasize the importance of isolating the causes of errors and uncertainties, such as soiling over the modules, which would indicate losses of up to 10%, according to the performed tests. Ndiaye et al. (2013) estimated the degradation of modules exposed for shorter periods (no more than four years), with initial rates of degradation ranging from 0.22% to almost 1% per year. Ishii and Masuda (2017) evaluated that LID caused an initial decrease of the power of the installed modules in the order of 2%, with a degradation rate around 0.2% per year after the stabilization period.

Other factors that difficult the evaluation of the degradation rate are due to the uncertainties associated to the measurement of the generator electric parameters. Typically, a good measurement of these parameters has uncertainty values lower than 2%. The irradiance is the major source of uncertainty and affects directly the short-circuit current. However, maximum power is the most sensitive parameter, because it suffers simultaneous interference from both irradiance and temperature, especially in outdoor measurements. Furthermore, the initial power degradation of the modules may be lower than the measurement uncertainty. Thus, long-term measurements, considering the accumulated degradation, are needed to achieve more significant results.

2. Photovoltaic generator characterization

The generator under study is constituted by consists of 48 modules installed onto the North façade of the UFRGS Solar Energy Laboratory building (as shown in Fig. 1), located in the city of Porto Alegre, Rio Grande do Sul, Brazil. The modules were made in Spain by ISOFOTON. This model (I-100/24), features 72 monocrystalline silicon (m-Si) cells, has the nominal characteristics of P_{MP} = 100 W_P, I_{SC} = 3.27 A and V_{OC} = 43.2 V, with dimensions of 1310 mm × 654 mm. The modules

Fig. 1. North façade of the LABSOL-UFRGS building.

were physically installed in two (upper and lower) lines of 24 modules each, inclined at 30° from the horizontal.

The nominal power of the system is 4.8 kW_P. The modules were electrically divided in three 1.6 kW_P arrays, each one formed by two strings of eight modules. The strings are interconnected in a box inside the building, which also houses the instrumentation sensors. The arrays, identified as East, Center and West, are connected to three corresponding single-phase inverters, injecting the converted energy into the three phase 220 V_{AC} grid.

Prior to the installation, the electrical parameters of every module were determined by measuring their *I-V* curves, thus allowing to the modules be classified and associated in the optimal operational configuration, minimizing mismatch losses (Krenzinger and Prieb, 2005). The installation was commissioned in 2004 and since then it has been intermittently monitored (Oliveira et al., 2018; Prieb and Krenzinger, 2007).

According to Koeppen (1948) the climate of the city of Porto Alegre (latitude −30.0° and longitude − 51.2°) is classified with Cfa (Humid temperate climate with hot summer). The average temperature is 19.6 °C, the average annual rainfall is 1397 mm and the average relative humidity is 76.5%. The global horizontal irradiation (GHI) is between 4.25 kWh/m^2·day and 4.50 kWh/m^2·day. In-plane of the modules (30°), the global irradiation is between 4.50 kWh/m^2·day and 4.75 kWh/m^2·day (Pereira et al., 2017).

3. Measurement aparatus and procedure

For the sake of better organization, the modules were identified according to their position in the installation using a two-letter code and a number. The first letter indicates the string horizontal position: E (East), C (Center) and W (West). The second letter indicates the vertical (line) position: H (high) or L (low). The number, ranging from 1 to 8 indicates the order of the module in the string. Number 1 informs the position farther left and 8, farther right. Therefore, code WL8, for example, indicates module 8 of the lower West string.

The electrical characterization from the *I-V* curve was conducted in all of the modules, as well as the visual inspection. The other tests (electroluminescence, thermography and electrical insulation) were applied to a sample of eight component modules from the lower west string.

Table 1 lists the most commonly reported defects in photovoltaic modules. It is possible to identify defects that may occur at different stages of the system operation. Some defects are typical of larger installations, such as PID, for example, caused by the high voltages resulting from the association of many modules in series. Other problems, such as cell discoloration, tend to happen in all modules, affecting the systems mostly after the first ten years of operation.

The aging of the modules and its influence on their electric behavior can be assessed in many ways and with different strategies. One can relate losses to the nominal value of the electrical parameters or to parameters taken from a non-degraded module (i.e., a reference module kept safe at the time of installation for future comparison) (Bouraiou et al., 2015; Kahoul et al., 2014). Kahoul et al. (2014) point out that small blackened burn points on the backsheet would indicate hot spots. However, García et al. (2013) indicate that hot-spots not always results in blackened points, so the visual inspection is not the proper tool for hot-spots identification.

3.1. Electrical characterization

The modules were electrically disconnected from the system and individually measured under natural sunlight, using a PVPM 1000C100 curve tracer. This equipment allows measuring either single modules, strings and arrays by selecting suitable voltage and current ranges according with the limits of these generators. The manufacturer declares that the electrical uncertainties for voltage and current measurements are less than 1% of the full scale of the measurement. Considering the voltage and current ranges used when measuring single modules (100 V and 10 A, respectively), the electrical uncertainty is less than 1 V for the voltage and less than 0.1 A for the current. The modules were carefully washed prior to the tests, in order to remove soiling and dirt, ensuring that the degradation assessment will take only permanent effects into consideration.

The temperature of the module under test during the *I-V* tracing was sensed by a Pt-100 attached to the backsheet at the central region of the module. The irradiance was sensed using a reference cell of m-Si installed at the same plane of the modules under test.

The measurements were carried out on days with clear sky, without any significant presence of clouds and with irradiances between 700 and 1000 W/m^2. The acquired *I–V* curves were translated to the standard condition using the method proposed by Bühler et al. (2014).

As mentioned before, all the modules had their individual *I-V* curves registered a few weeks prior to the installation in 2004, as described in Krenzinger and Prieb (2005). In order to evaluate the main electrical parameters influenced by the degradation, the raw data from these measurements was retrieved and translated to standard conditions using the same method applied to the new measurements. The instrumentation used in these tests was described in Prieb (2002). Uncertainties for voltage and current measurements were of ± 0.01 V and ± 0.02 A, respectively.

Additionally, it was registered the *I-V* curve of an array constituted by 16 modules, formed by the CL and WL strings connected in parallel. *I-V* curves of this array were taken in 2006 (Prieb and Krenzinger, 2007) and 2017 (Oliveira et al., 2018). These are the only available *I-V* curves of this array prior to this paper, as only individual curves were taken in 2004. The instrumentation employed in 2006 is the same described in Prieb (2002), with the electronic load replaced with a variable resistive load. 2017 curves were taken with an EKO MP-11 a curve tracer (electrical uncertainties of 6 V and 0.1 A, considering the ranges used in the tests). All curves were translated to standard conditions using the same method applied in all the measurements.

The next step was to submit the modules to the insulation test described in IEC 61215-1 (2016). Eight modules were selected for this and other specific tests, taken from a string located at the west side of the system structure. Lorenzo et al. (2013) points out that this type of test is not commonly performed on field exposed modules.

3.2. Electroluminescence and visual inspection

The analysis of the modules electrical performance allows the quantitative evaluation of the main degradation modes. However, other methods can serve also as a tool to detect photovoltaic modules degradation. Thus, in addition to the electrical characterization, qualitative tests such as visual inspection, electroluminescence and thermal imaging were also performed.

Table 1
Degradation modes identification.

Degradation mode	Evaluation	Reference
EVA browning	Visual/I_{SC}	Czanderna and Pern (1996) and Ndiaye et al. (2013)
Backsheet delamination	Visual/Electrical Insulation	Lorenzo et al. (2013)
Internal circuitry corrosion (series resistance increase	*I-V* Curve/R_S/Visual/EL	Jordan et al. (2017) and Zhu et al. (2016)
Cell delamination	Visual	Sánchez-Friera et al. (2011)
Anti-Reflective coating defects	Visual	Munoz et al. (2011)
Hot-spots	Termography/*I-V* Curve	García et al. (2013) and Rajput et al. (2016a,b)
Broken cells	Visual/EL/*I-V* Curve	Köntges et al. (2014) and Meyer and van Dyk (2004)
Diode/j-box problem	Visual	Lorenzo et al. (2013)
Glass breakage	Visual	Ndiaye et al. (2013)
PID	*I-V* Curve/EL/Termography	Bedrich et al. (2018) and Harvey et al. (2016) and Martinez-Moreno et al. (2013)
Frame deformation	Visual	Köntges et al. (2014)

Visual inspection is an essential tool for identifying different apparent defects, such as cell cracks and encapsulant discoloration. In order to track an eventual defect evolution, it is very important to record any abnormalities found, even if they affect minimally (or not at all) the electrical behavior of the modules. It is convenient to keep a record with good images of the module, registering the defects dimension and other relevant information (Köntges et al., 2014). The visual inspection was done on all of the 48 modules.

In EL test modules are forward biased with a current in the order of I_{SC}. The recombination of electron-hole pairs results in a low intensity emission. As the emitted radiation occurs at near IR range (between the wavelengths of 1000 nm and 1300 nm), a camera with a suitable sensor is required. While specific cameras are commercially available, it is possible to use an adapted conventional camera, as described by Figueiredo et al. (2018). Since EL tests require a dark environment, indoor testing is generally easier to conduct. Nevertheless, it can be performed outdoor under certain field conditions (Koch et al., 2016).

3.3. Thermal imaging

Thermographic images were also taken in order to perform a thermal analysis of the modules. Thermographic imaging is referred in the literature as a tool for detecting defects such as operational mismatch (Sánchez-Friera et al., 2011), hot spots (García et al., 2013) and even PID (Martinez-Moreno et al., 2013). Furthermore, field thermography is useful for observing temperature distribution in the modules. The camera used for inspection was a THERMOCOM V52 with proprietary software for post-processing, analysis and reporting.

3.4. Electrical insulation test

According to IEC 61215-1 (2016), insulation testing aims to verify insulation between the live and accessible parts of the PV module. To be approved, the module should not suffer dielectric breakdown or show surface tracking. The insulation resistance must be equal to or greater than 400 MΩ for modules of area less than 0.1 m^2. For modules with area larger than 0.1 m^2 the product resistance per area must be equal to or greater than 40 MΩ·m^2.

4. Results and discussion

4.1. Electrical characterization

The histograms in Fig. 2 were built with the data from the *I-V* curves taken in 2004. These curves were measured with irradiance between 940 and 1070 W/m^2 and cell temperature between 53 and 64 °C, later translated to the standard condition. In the figure, (a) represents the maximum power, (b) the short circuit current, (c) the open circuit voltage and (d) the fill factor.

Similar histograms, shown in Fig. 3 were made from the *I-V* curves obtained after 15 years of operation. They represent the dispersion of the electrical parameters of the modules after affected by some type of degradation. Again, (a) represents the maximum power, (b) the short circuit current, (c) the open circuit voltage and (d) the fill factor.

Analyzing the histogram of V_{OC} in Fig. 3, one can notice a module that has a much lower voltage, about 2/3 of the other modules. This particular module, which *I-V* curve is shown in Fig. 4, was found to have two of its six series of cells inactive due to a failure in an internal connection. This failure was probably caused by moisture penetration, since this particular module (identified as EL6, the sixth module of the lower east string) had its junction box detached from the backsheet. Thus, for the analysis of degradation after 15 years of operation, this module was discarded and only 47 modules were considered.

Table 2 shows the mean values of the electrical parameters extracted from the 2004 and 2019 sets of *I–V* curves and the corresponding standard deviations. The average maximum power has decreased by 9.50%, mostly due to current reduction (9.19% and 9.12% for I_{MP} and I_{SC}, respectively). The other parameters (V_{OC}, V_{MP} and *FF*) did not present significant variation. The annual average power degradation is in the order of 0.7%. It was observed a significant increase in the dispersion of the short circuit and maximum power currents (and consequently the maximum power), suggesting a greater mismatch of the electrical parameters between the modules when compared to the mismatch observed before 15 years of operation.

Considering the standard deviation normalized by the mean, the relative standard deviation of the maximum power current is 1.06% for modules before installation and 2.72% after 15 years. As described in Krenzinger and Prieb (2005), the modules were classified according to the maximum power current and voltage prior to installation in order to minimize power loss due to electrical mismatch. The authors concluded that using this selection criterion resulted in 2.5% more power than if the modules were selected randomly. However, one has to take into account that tracing the *I-V* curves of all the modules is a costly and time consuming task, so the effort may be worthwhile, even more when considered the tighter specifications of nowadays modules.

Fig. 5 shows the *I-V* curve of the module EH1 that presented smallest power reduction and Fig. 6 shows the *I-V* curve of the module CL1 that presented largest power reduction.

Fig. 7 shows three *I-V* curves of array formed by CL and WL strings connected in parallel taken in 2006, 2017 and 2019.In the graph it is possible to evaluate the power decrease over the years. Table 3 presents the electrical parameters taken from the same curves.

4.2. Thermographic inspection

Fig. 8 shows thermographic images of the lower West string. During the days of the inspection, the temperature difference from cell to cell was less than 3 °C, except for the region over the junction boxes. The same behavior was also observed in the other modules of the system. Given the homogeneous temperature distribution over the modules, measuring the temperature at a single point of the module did not introduce significant errors. Due to the low system voltages (under

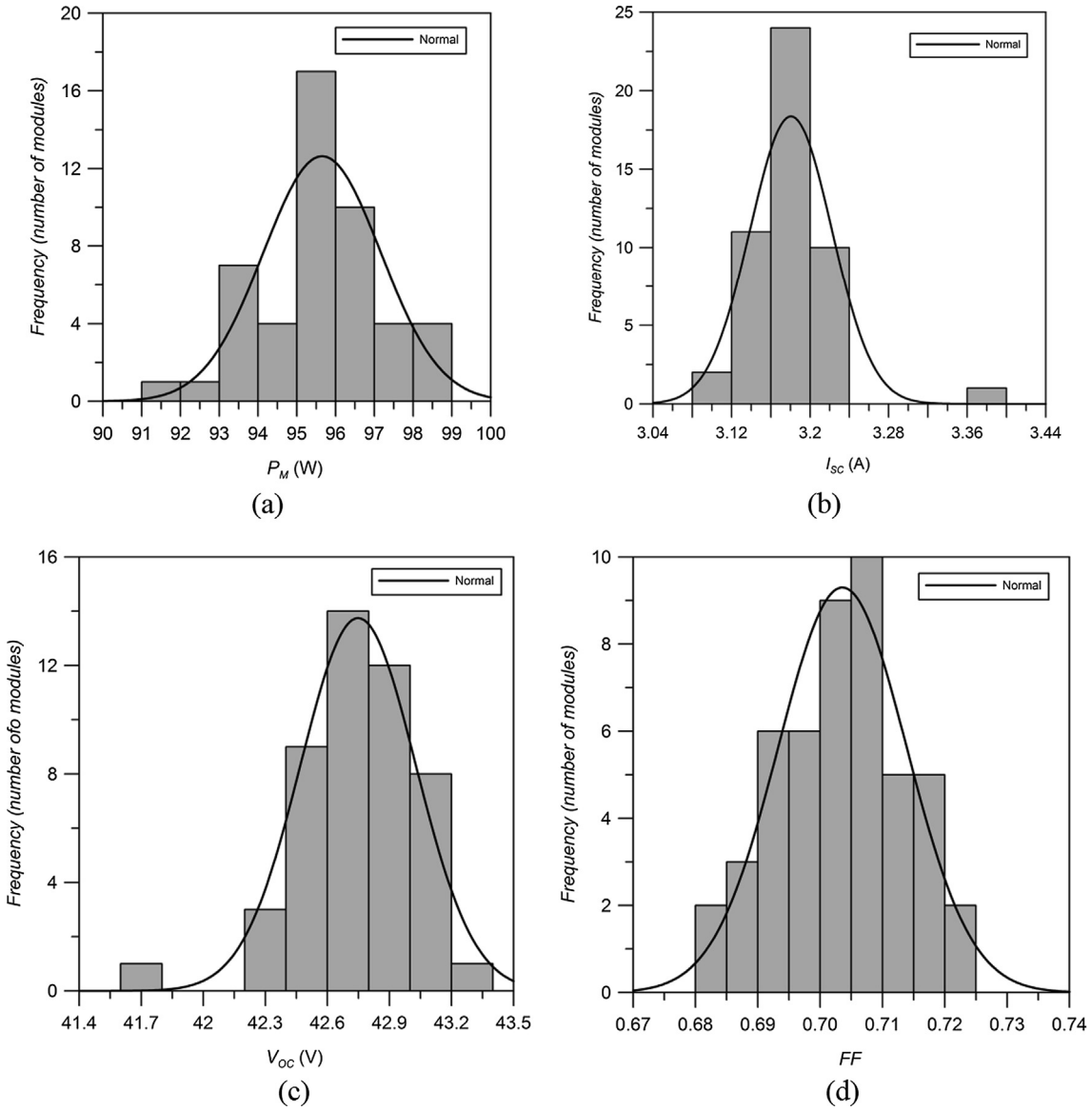

Fig. 2. Dispersion of the electric parameters before installation: (a) maximum power, (b) short circuit current, (c) open circuit voltage and (d) fill factor.

350 V), the existence of PID (which could also be detected by a non-uniform distribution in operating temperature as mentioned by Martinez-Moreno et al., 2013) was not considered.

In Fig. 8, the temperature gauge was fitted from 40 °C to 50 °C, the temperatures on the glass cover were corrected using the methodology presented by Krenzinger and de Andrade (2007) ranging from 43 to 49 °C. A hotter area can be observed in one of the modules. This module (EL6), presented an inactive area as revealed by its *I-V* curve (Fig. 4).

4.3. Electrical insulation

The IEC 61215-1 (2016) standard defines the voltage to be applied in the electrical insulation test as twice the maximum system voltage plus 1000 V. In this case, the maximum system voltage is 750 V, so the applied voltage was 2500 V. Considering the surface area of the modules of 0.857 m^2, the measured insulation resistance must be equal to or greater than 46.69 MΩ.

Table 4 shows the results for the eight tested samples. All modules passed the test.

4.4. Visual inspection results

Visual inspection is also described in IEC 61215-1 (2016). Commonly reported problems such as bubble formation, busbar corrosion, frame deformation, terminal box breakage, delamination, and backsheet disintegration were not addressed in this visual inspection.

After 15 years of operation, EVA darkening affected 100% of the module cells. Another problem that was also vastly observed is the frontal delamination of the cells, forming a milky pattern. Other observed phenomenon that may be associated with encapsulant decomposition is the oxidation of the anti-reflective layer. Figs. 9–13 show the main degradation modes obtained through visual inspection.

Fig. 9 details a region of CH3 module, featuring frontal delamination and early formation of milky pattern. Fig. 10 shows the region of module CL6 with formation of milky pattern. These occurrences are similar to those identified in (Bouraiou et al., 2015; Sánchez-Friera et al., 2011).

Fig. 11 shows the delamination between glass and encapsulant in module CL7. This defect is similar to that shown in Tang et al. (2006). Fig. 12 shows deterioration of the anti-reflective layer at the edges of one module WH3 cell, other important effect that occurs as a

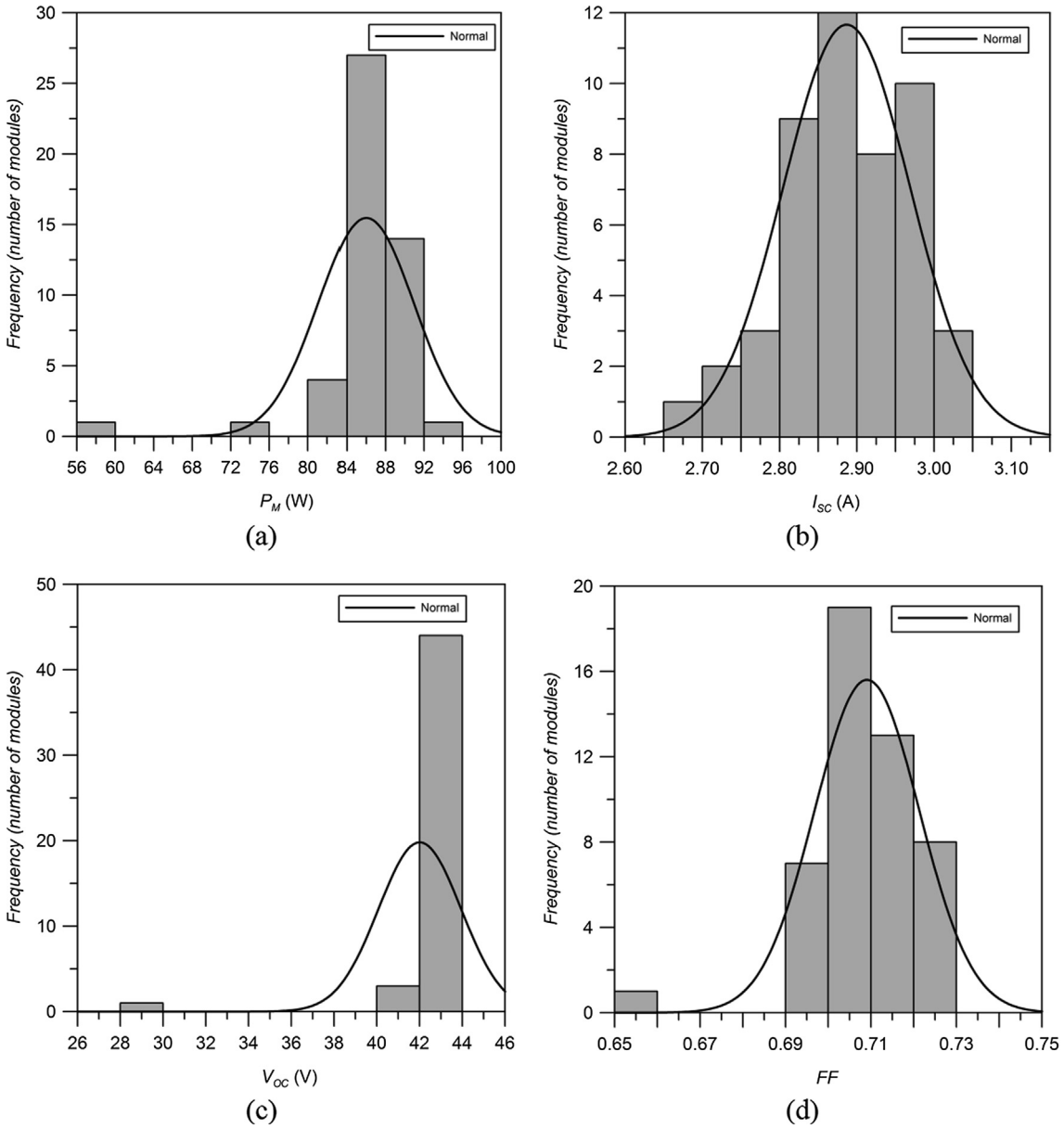

Fig. 3. Dispersion of the electric parameters after 15 years of operation: (a) nominal power, (b) short circuit current, (c) open circuit voltage and (d) fill factor.

consequence of delamination.

Fig. 13 shows the deterioration of the anti-reflective layer on a WL6 module cell, similar as found in Munoz et al. (2011).

From just the visual inspection it was possible to summarize the main degradation modes and their significance on the installation under study.

Table 5 indicates the various types of defects found in the installation ranked by frequency of incidence. Were also included the defects most commonly observed in other PV generators that have not been observed, at least so far, in the system under study.

Table 5 shows that the degradation modes were evaluated and identified by complementary analysis, such as the *I-V* curve. The disconnection of a set of EL6 module cells was not observed at the first visual assessment. Other complementary analysis revealed that the diodes, including those in the module that operated with lower voltage, were operational.

4.5. Electroluminescence results

To complement the analysis, the modules were submitted to electroluminescence test. This technique allows the identification of totally or partially inactive cells. All cracked cells previously identified by visual inspection were confirmed by the electroluminescence technique.

Fig. 14 shows the EL image of the faulty module EL6. Since thins module had at least one of its internal connections open, this image was only possible to be obtained by bypassing the diode corresponding to the set of disconnected cells.

Figs. 15 and 16 show the EL images of modules WL1 and WL3, respectively, in which can be observed cells with operational mismatch in relation to the others. This effect can be detected from the higher intensity of emitted radiation, due to the fact that the defective cell has a smaller active region. In Zhu et al. (2016), a similar effect was demonstrated when observing EL images of modules submitted to damp heat test.

The EL images can reveal electrically inactive regions in cells. The appearance of these regions may be result of the action of some

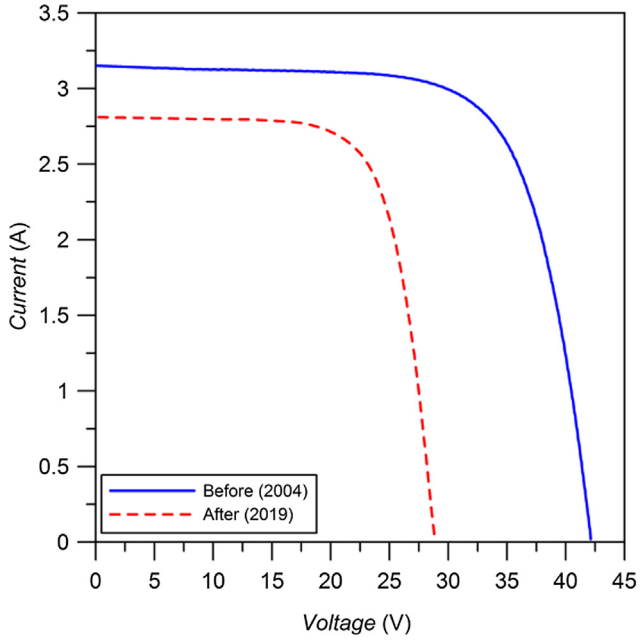

Fig. 4. Measured *I-V* curves of module EL6, as new and after 15 years of operation.

Table 2
Average and standard deviation of the characteristics parameters of the PV modules, before and after 15 years of operation.

	Initial Measurement		Final Measurement		Variation	
	μ	σ	μ	σ	μ (%)	σ (%)
I_{SC} (A)	3.18	0.04	2.89	0.08	−9.12	+100
V_{OC} (V)	42.76	0.27	42.29	0.22	−1.10	−18.52
I_{MP} (A)	2.83	0.03	2.57	0.07	−9.19	+133.33
V_{MP} (V)	33.77	0.37	33.65	0.38	−0.36	+2.70
P_M (W)	95.69	1.53	86.60	2.86	−9.50	+86.93
FF (%)	70.35	1.05	70.89	1.25	+0.77	+19.61

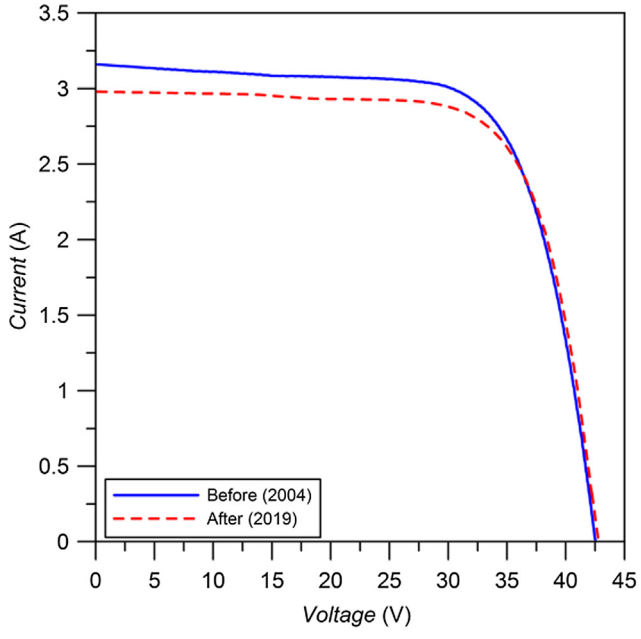

Fig. 5. Measured *I-V* curve of the module EH1 that presented smallest power reduction.

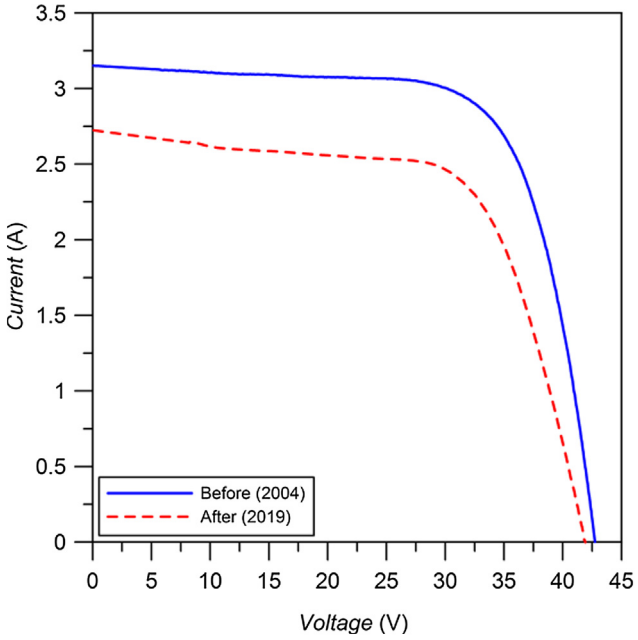

Fig. 6. *I-V* curve of the module CL1 that presented largest power reduction.

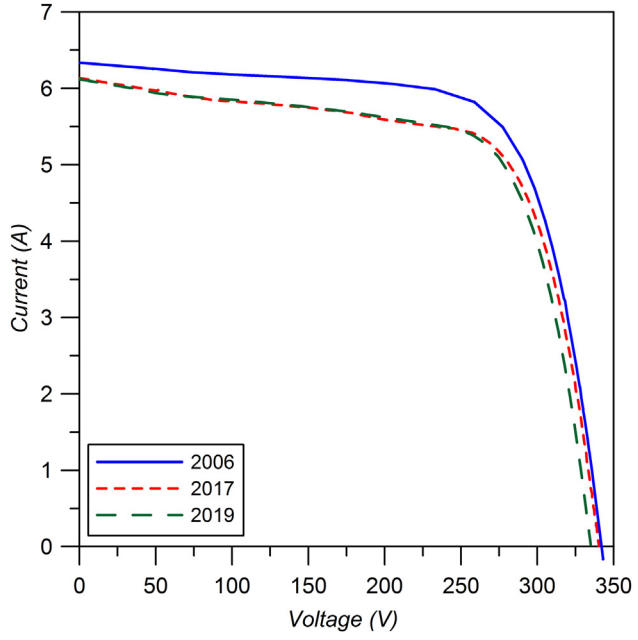

Fig. 7. *I-V* curves of the array made from CL and WL strings.

Table 3
Electrical parameters of the PV array in 2006, 2017 and 2019.

	2006	2017	2019
I_{SC} (A)	6.34	6.13	6.11
V_{OC} (V)	342.11	340.89	335.01
I_{MP} (A)	5.61	5.21	5.24
V_{MP} (V)	272.33	273.04	268.81
P_M (W)	1527.22	1422.89	1407.26
FF (%)	70.44	68.04	68.75

degradation mechanism, for example, corrosion of the cell contacts (Zhu et al., 2016) or shunted areas (Bedrich et al., 2018; Harvey et al., 2016).

Fig. 17 depicts ordinary and EL images of the brightest cell of WL1

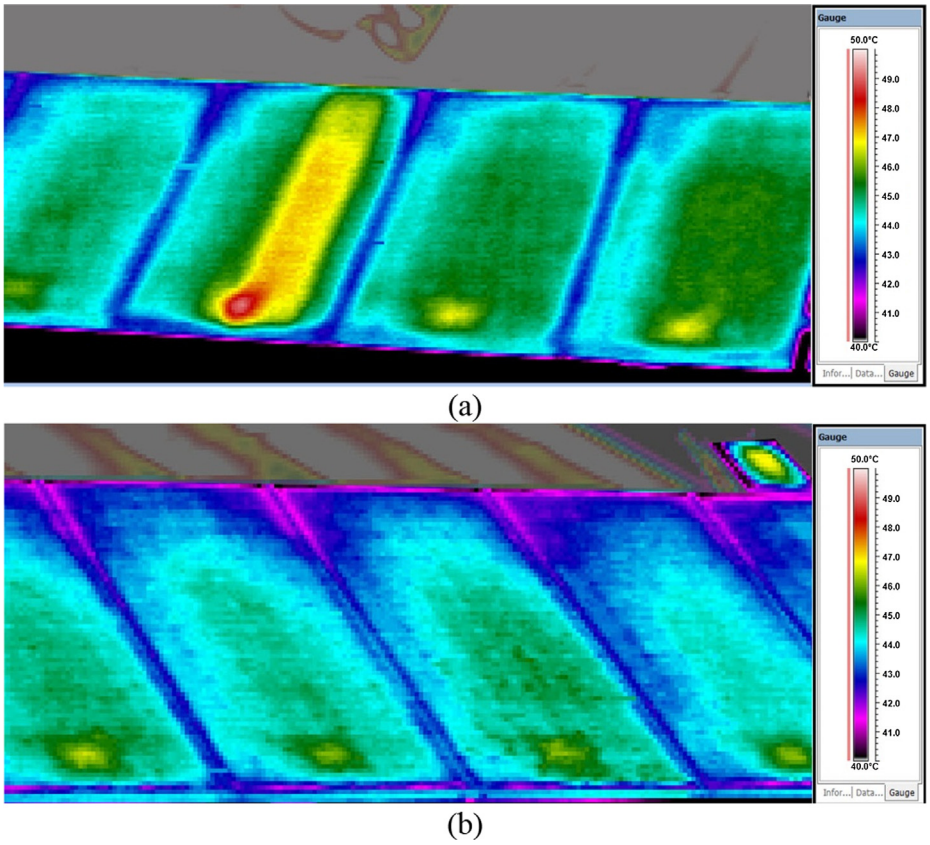

Fig. 8. Thermographic images of inferior arrays, (a) East and (b) West.

Table 4
Electrical insulation test.

Identification	R_{ISO} (MΩ)
WL1	1265
WL2	1265
WL3	2500
WL4	500
WL5	625
WL6	625
WL7	1265
WL8	1265

Fig. 9. Detail of CH3 module presenting frontal delamination and early formation of milky pattern.

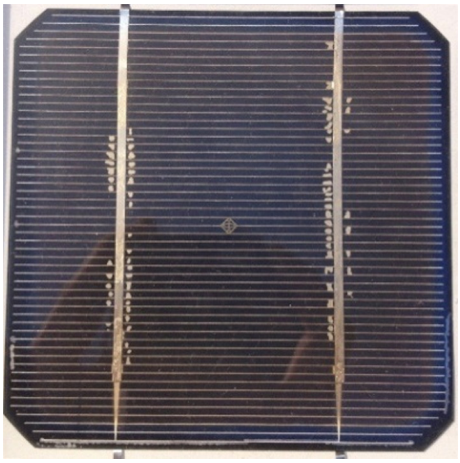

Fig. 10. CL6 module seriously affected by milky pattern formation.

module. The regular photograph (a) shows no apparent indication of a problem in the cell that justifies the inactive region shown in the EL image (b).

5. Conclusion

The aging of a 48-module system operating for 15 years in the city of Porto Alegre was analyzed using techniques previously described in studies on photovoltaic module degradation. Visual inspection revealed that all modules already had some problems related to their aging. Darkening of the encapsulant, as well as oxidation of the anti-reflective layer, was observed in all modules. The presence of milky pattern was verified in 38 modules and 13 presented broken cells. Thermographic images did not reveal hot spots. One module presented an atypical

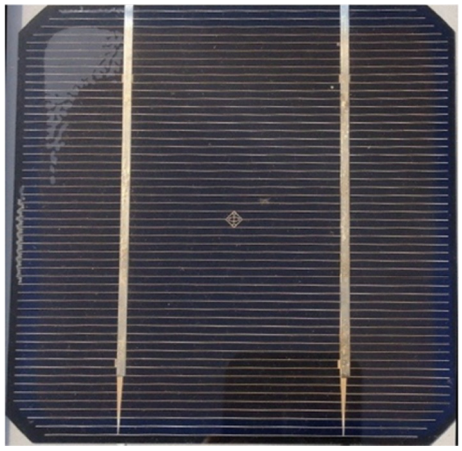

Fig. 11. Delamination between glass and encapsulant in module CL7.

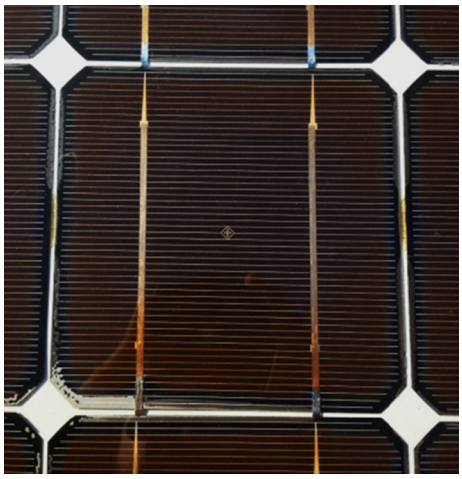

Fig. 12. Deterioration of the anti-reflective layer at the edges of a WH3 module cell.

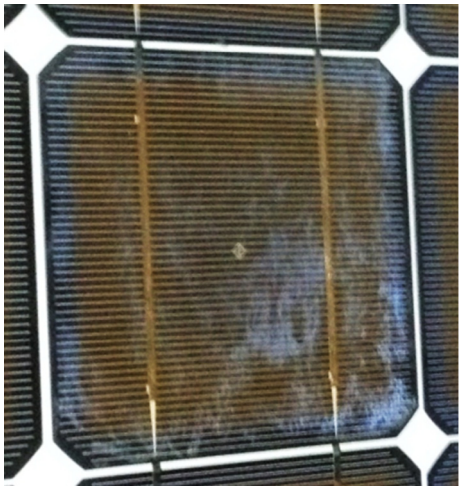

Fig. 13. Deterioration of the anti-reflective layer in a WL6 module cell.

electrical behavior. Further tests indicated that some internal electrical joint was defective, causing 24 of its 72 cells to not operate properly.

The electrical characterization from the *I-V* curve data, obtained before and after the 15-year period for each of the 48 modules, indicates 9.50% loss in the average installation power, corresponding to a yearly average of 0.7%. This power loss was mostly due to current

Table 5
Type of defects found.

Type of Defect	Incidence			
	Modules	%	Cells	%
Browning	48	100	3456	100
Anti-reflective coating oxidation	48	100	3456	100
Milky pattern	38	79.2	2736	79.2
Cell cracks	13	27.1	18	0.5
Backsheet delamination	1	2.1	24	0.7
Contact corrosion	1	2.1	24	0.7
Defective By-pass diodes	0	0	0	0
Hot-spots	0	0	0	0

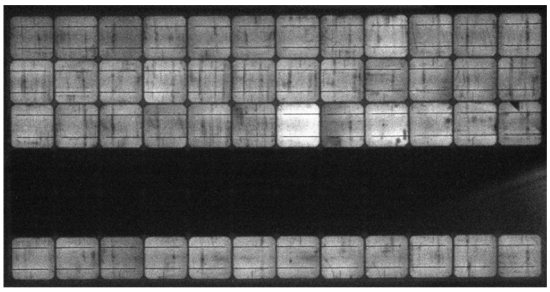

Fig. 14. EL image of module EL6.

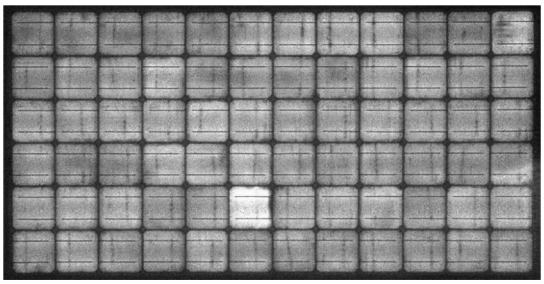

Fig. 15. EL image of WL1 module.

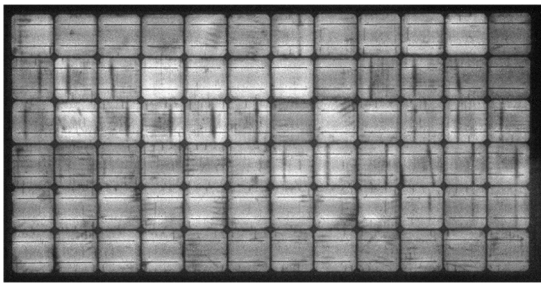

Fig. 16. EL image of WL3 module.

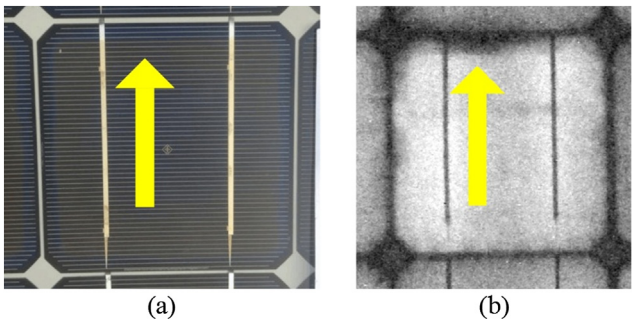

Fig. 17. Regular and EL images of WL1 module's brightest cell.

reduction (9.19% and 9.12% for I_{MP} and I_{SC}, respectively).

The low variation in the fill factor (0.77%) suggests that there were no significant changes in the series resistance. The EL images revealed inactive regions in the periphery of the cells, indicating the action of some degradation mechanism undetectable to the naked eye. These defects, along with the encapsulant darkening and the anti-reflective layer degradation, contribute significantly to the reduction of short circuit current.

Declaration of Competing Interest

The authors declare that they have no known competing financial interests or personal relationships that could have appeared to influence the work reported in this paper.

Acknowledgments

This work was financially supported by CNPq (Conselho Nacional de Desenvolvimento Científico e Tecnológico), by the Coordenação de Aperfeiçoamento de Pessoal de Nível Superior – Brasil (CAPES) – Finance Code 001 and Erasmus Mundus Programme SMART2 Project: SmartCities & SmartGrids for Sustainable Development.

References

Bedrich, K.G., Luo, W., Pravettoni, M., Chen, D., Chen, Y., Wang, Z., Verlinden, P.J., Hacke, P., Feng, Z., Chai, J., Wang, Y., Aberle, A.G., Khoo, Y.S., 2018. Quantitative electroluminescence imaging analysis for performance estimation of PID-influenced PV modules. IEEE J. Photovolt. 8, 1281–1288. https://doi.org/10.1109/JPHOTOV.2018.2846665.

Berardone, I., Lopez Garcia, J., Paggi, M., 2018. Analysis of electroluminescence and infrared thermal images of monocrystalline silicon photovoltaic modules after 20 years of outdoor use in a solar vehicle. Sol. Energy 173, 478–486. https://doi.org/10.1016/J.SOLENER.2018.07.055.

Bouraiou, A., Hamouda, M., Chaker, A., Mostefaoui, M., Lachtar, S., Sadok, M., Boutasseta, N., Othmani, M., Issam, A., 2015. Analysis and evaluation of the impact of climatic conditions on the photovoltaic modules performance in the desert environment. Energy Convers. Manag. 106, 1345–1355. https://doi.org/10.1016/J.ENCONMAN.2015.10.073.

Bühler, A.J., Perin Gasparin, F., Krenzinger, A., 2014. Post-processing data of measured I-V curves of photovoltaic devices. Renew. Energy 68, 602–610. https://doi.org/10.1016/j.renene.2014.02.048.

Chandel, S.S., Nagaraju Naik, M., Sharma, V., Chandel, R., 2015. Degradation analysis of 28 year field exposed mono-c-Si photovoltaic modules of a direct coupled solar water pumping system in western Himalayan region of India. Renew. Energy 78, 193–202. https://doi.org/10.1016/J.RENENE.2015.01.015.

Czanderna, A.W., Pern, F.J., 1996. Encapsulation of PV modules using ethylene vinyl acetate copolymer as a pottant: a critical review. Sol. Energy Mater. Sol. Cells 43, 101–181. https://doi.org/10.1016/0927-0248(95)00150-6.

Jordan, D.C., Wohlgemuth, J.H., Kurtz, S.R., 2012. Technology and climate trends in PV module degradation. In: Proceedings of the 27th European Photovoltaic Solar Energy Conference and Exhibition, pp. 3118–3124. https://doi.org/10.4229/27thEUPVSEC2012-4DO.5.1.

Figueiredo, G., Almeida, M.P., Manito, A., Zilles, R., 2018. Alternativa de baixo custo para imagens em eletroluminescência de módulos fotovoltaicos. VII Congresso Brasileiro de Energia Solar.

García, M., Marroyo, L., Lorenzo, E., Marcos, J., Pérez, M., 2013. Observed degradation in photovoltaic plants affected by hot-spots. Prog. Photovolt. Res. Appl. 22, 1292–1301. https://doi.org/10.1002/pip.2393.

Harvey, S.P., Aguiar, J.A., Hacke, P., Guthrey, H., Johnston, S., Al-Jassim, M., 2016. Sodium accumulation at potential-induced degradation shunted areas in polycrystalline silicon modules. IEEE J. Photovolt. 6, 1440–1445. https://doi.org/10.1109/JPHOTOV.2016.2601950.

IEA, 2019. Snapshot of Global Photovoltaic Markets – 2019.

IEC 61215-1, 2016. International Electrotechnical Commission. Terrestrial photovoltaic (PV) modules – Design qualification and type approval – Part 1-1: Special requirements for testing of crystalline silicon photovoltaic (PV) modules.

Ishii, T., Masuda, A., 2017. Annual degradation rates of recent crystalline silicon photovoltaic modules. Prog. Photovolt. Res. Appl. 25, 953–967. https://doi.org/10.1002/pip.2903.

Jordan, D.C., Kurtz, S.R., 2013. Photovoltaic degradation rates-an analytical review. Prog. Photovolt. Res. Appl. 21, 12–29. https://doi.org/10.1002/pip.1182.

Jordan, D.C., Silverman, T.J., Wohlgemuth, J.H., Kurtz, S.R., VanSant, K.T., 2017. Photovoltaic failure and degradation modes. Prog. Photovolt. Res. Appl. 25, 318–326. https://doi.org/10.1002/pip.2866.

Jorgensen, G.J., McMahon, T.J., 2008. Accelerated and outdoor aging effects on photovoltaic module interfacial adhesion properties. Prog. Photovolt. Res. Appl. 16, 519–527. https://doi.org/10.1002/pip.826.

Kahoul, N., Houabes, M., Sadok, M., 2014. Assessing the early degradation of photovoltaic modules performance in the Saharan region. Energy Convers. Manag. 82, 320–326. https://doi.org/10.1016/J.ENCONMAN.2014.03.034.

Koch, S., Weber, T., Sobottka, C., Fladung, A., Clemens, P., Berghold, J., 2016. Outdoor electroluminescence imaging of crystalline photovoltaic modules: comparative study between manual ground-level inspections and drone-based aerial surveys. In: 32nd European Photovoltaic Solar Energy Conference and Exhibition, pp. 1736–1740. https://doi.org/10.4229/EUPVSEC20162016-5DO.12.2.

Koeppen, W., 1948. Climatología: Con un estudio de los climas de la Tierra. Fondo de Cultura Economica.

Köntges, M., Kurtz, S.R., Packard, C., Jahn, U., Berger, K.A., Kato, K., Friesen, T., Liu, H., Iseghem, M. Van, 2014. Review of Failures of Photovoltaic Modules.

Krenzinger, A., de Andrade, A.C., 2007. Accurate outdoor glass thermographic thermometry applied to solar energy devices. Sol. Energy 81, 1025–1034. https://doi.org/10.1016/j.solener.2006.11.014.

Krenzinger, A., Prieb, C.W.M., 2005. Clasificación y selección de módulos fotovoltaicos para una central conectada a la red. Av. en Energías Renov. y Medio Ambient. 9 04.19–04.24.

Larocca, M.T.M., 2013. Degradación de módulos fotovoltaicos: análisis desde el punto de vista eléctrico y su interrelación con otros factores. Universidad Nacional de Salta.

Lorenzo, E., Zilles, R., Moretón, R., Gómez, T., Martínez de Olcoz, A., 2013. Performance analysis of a 7-kW crystalline silicon generator after 17 years of operation in Madrid. Prog. Photovolt. Res. Appl. 22, 1273–1279. https://doi.org/10.1002/pip.2379.

Martinez-Moreno, F., Lorenzo, E., Munoz, J., Parra, R., Espino, T., 2013. On site tests for the detection of potential induced degradation in modules. In: 28th European Photovoltaic Solar Energy Conference and Exhibition, pp. 3313–3317. https://doi.org/10.4229/28thEUPVSEC2013-4AV.5.43.

Meyer, E.L., van Dyk, E.E., 2004. Assessing the reliability and degradation of photovoltaic module performance parameters. IEEE Trans. Reliab. 53, 83–92. https://doi.org/10.1109/TR.2004.824831.

Moretón, R., Lorenzo, E., Narvarte, L., 2015. Experimental observations on hot-spots and derived acceptance/rejection criteria. Sol. Energy 118, 28–40. https://doi.org/10.1016/j.solener.2015.05.009.

Munoz, M.A., Alonso-García, M.C., Vela, N., Chenlo, F., 2011. Early degradation of silicon PV modules and guaranty conditions. Sol. Energy 85, 2264–2274. https://doi.org/10.1016/j.solener.2011.06.011.

Ndiaye, A., Charki, A., Kobi, A., Kébé, C.M.F., Ndiaye, P.A., Sambou, V., 2013. Degradations of silicon photovoltaic modules: a literature review. Sol. Energy 96, 140–151. https://doi.org/10.1016/j.solener.2013.07.005.

Oliveira, F.S., Soares, L.D.M., Prieb, C.W.M., Krenzinger, A., 2018. Avaliação de um arranjo fotovoltaico após onze anos de operação. VII Congresso Brasileiro de Energia Solar. Associação Brasileira de Energia Solar, Gramado/Brasil.

Osterwald, C.R., McMahon, T.J., 2009. History of accelerated and qualification testing of terrestrial photovoltaic modules: a literature review. Prog. Photovolt. Res. Appl. 17, 11–33. https://doi.org/10.1002/pip.861.

Osterwald, C.R., Pruett, J., Moriarty, T., 2005. Crystalline silicon short-circuit current degradation study: initial results. In: Conference Record of the Thirty-First IEEE Photovoltaic Specialists Conference. IEEE, Lake Buena Vista, FL, USA, pp. 1335–1338. https://doi.org/10.1109/PVSC.2005.1488388.

Pereira, E.B., Martins, F.R., Gonçalves, A.R., Costa, R.S., de Lima, F.J.L., Rüther, R., de Abreu, S.L., Tiepolo, G.M., Pereira, S.V., de Souza, J.G., 2017. Atlas Brasileiro de Energia Solar, 2nd ed. INPE, São José dos Campos.

Pern, F.J., 1996. Factors that affect the EVA encapsulant discoloration rate upon accelerated exposure. Sol. Energy Mater. Sol. Cells 41–42, 587–615. https://doi.org/10.1016/0927-0248(95)00128-X.

Pingel, S., Koshnicharov, D., Frank, O., Geipel, T., Zemen, Y., Striner, B., Berghold, J., 2010. Initial degradation of industrial silicon solar cells in solar panels. In: 25th European Photovoltaic Solar Energy Conference and Exhibition/5th World Conference on Photovoltaic Energy Conversion. Valencia, Spain, pp. 4027–4032. https://doi.org/10.4229/25thEUPVSEC2010-4AV.3.20.

Polverini, D., Field, M., Dunlop, E., Zaaiman, W., 2012. Polycrystalline silicon PV modules performance and degradation over 20 years. Prog. Photovolt. Res. Appl. 21, 1004–1015. https://doi.org/10.1002/pip.2197.

Prieb, C.W.M., 2002. Desenvolvimento de um Sistema de Ensaio de Módulos Fotovoltaicos. Universidade Federal do Rio Grande do Sul, Porto Alegre.

Prieb, C.W.M., Krenzinger, A., 2007. Determinação de curva característica de arranjo fotovoltaico. CBENS - I Congresso Brasileiro de Energia Solar. Associação Brasileira de Energia Solar, Fortaleza.

Rajput, P., Tomar, V., Tiwari, G.N., Sastry, O.S., Bhatti, T.S., 2018. A thermal model for N series connected glass/cell/polymer sheet and glass/cell/glass crystalline silicon photovoltaic modules with hot solar cells connected in series and its thermal losses in real outdoor condition. Renew. Energy 126, 370–386. https://doi.org/10.1016/J.RENENE.2018.03.040.

Rajput, P., Tiwari, G.N., Sastry, O.S., 2016a. Thermal modelling and experimental validation of hot spot in crystalline silicon photovoltaic modules for real outdoor condition. Sol. Energy 139, 569–580. https://doi.org/10.1016/j.solener.2016.10.016.

Rajput, P., Tiwari, G.N., Sastry, O.S., Bora, B., Sharma, V., 2016b. Degradation of monocrystalline photovoltaic modules after 22 years of outdoor exposure in the composite climate of India. Sol. Energy 135, 786–795. https://doi.org/10.1016/j.solener.2016.06.047.

REN21, 2018. Renewables 2018 Global Status Report, Global Status Report.

Sánchez-Friera, P., Piliougine, M., Peláez, J., Carretero, J., Sidrach de Cardona, M., 2011. Analysis of degradation mechanisms of crystalline silicon PV modules after 12 years of operation in Southern Europe. Prog. Photovolt. Res. Appl. 19, 658–666. https://doi.org/10.1002/pip.1083.

Schweiger, M., Bonilla, J., Herrmann, W., Gerber, A., Rau, U., 2017. Performance stability

of photovoltaic modules in different climates. Prog. Photovolt. Res. Appl. 25, 968–981. https://doi.org/10.1002/pip.2904.
Skoczek, A., Sample, T., Dunlop, E.D., 2009. The results of performance measurements of field-aged crystalline silicon photovoltaic modules. Prog. Photovolt. Res. Appl. 17, 227–240. https://doi.org/10.1002/pip.874.
Solórzano, J., Egido, M.A., 2013. Automatic fault diagnosis in PV systems with distributed MPPT. Energy Convers. Manag. 76, 925–934. https://doi.org/10.1016/J.ENCONMAN.2013.08.055.
SPA, 2018. Global Market Outlook for Solar Power 2018–2022. Global Market Outlook.
Tang, Y., Raghuraman, B., Kuitche, J., TamizhMani, G., Backus, C.E., Osterwald, C., 2006. An evaluation of 27 + years old photovoltaic modules operated in a hot-desert climatic condition. In: 2006 IEEE 4th World Conference on Photovoltaic Energy Conference. IEEE, pp. 2145–2147. https://doi.org/10.1109/WCPEC.2006.279929.
Vera, L.H., Prieb, C.W.M., Krenzinger, A., 2006. Comparação do Desempenho de Módulos Fotovoltaicos Após Seis Anos de Operação. Av. en Energías Renov. y Medio Ambient. 10, 25–36.
Wohlgemuth, J.H., Kurtz, S., 2011. Reliability testing beyond Qualification as a key component in photovoltaic's progress toward grid parity. In: 2011 International Reliability Physics Symposium. IEEE, pp. 5E.3.1–5E.3.6. https://doi.org/10.1109/IRPS.2011.5784534.
Zhu, J., Koehl, M., Hoffmann, S., Berger, K.A., Zamini, S., Bennett, I., Gerritsen, E., Malbranche, P., Pugliatti, P., Di Stefano, A., Aleo, F., Bertani, D., Paletta, F., Roca, F., Graditi, G., Pellegrino, M., Zubillaga, O., Iranzo, F.J.C., Pozza, A., Sample, T., Gottschalg, R., 2016. Changes of solar cell parameters during damp-heat exposure. Prog. Photovolt. Res. Appl. 24, 1346–1358. https://doi.org/10.1002/pip.2793.